8-2024

Patterning Synthesis of Lead Halide Perovskites Toward Photonic Application

S. M. Nayeem Arefin
University of Nebraska-Lincoln, narefin2@huskers.unl.edu

PATTERNING SYNTHESIS OF LEAD HALIDE PEROVSKITES TOWARD PHOTONIC APPLICATION

by

S M Nayeem Arefin

A THESIS

Presented to the Faculty of

The Graduate College at the University of Nebraska

In Partial Fulfillment of Requirements

For the Degree of Master of Science

Major: Electrical Engineering

Under the Supervision of Professor Yanan (Laura) Wang

Lincoln, Nebraska

August 2024

PATTERNING SYNTHESIS OF LEAD HALIDE PEROVSKITES TOWARD PHOTONIC APPLICATION

S M Nayeem Arefin, MS

University of Nebraska, 2024

Advisor: **Yanan (Laura) Wang**

Lead halide perovskites (LHPs) are a fascinating class of photonic materials with the potential to revolutionize various optoelectronic applications. Their diverse crystal structures, ranging from 0D to 3D configurations, offer a unique combination of properties, including high tunability and ease of synthesis. However, their inherent instability and the difficulty of patterning them into sophisticated photonic structures using conventional methods present a significant hurdle to their widespread applications. This thesis addresses these challenges by proposing a novel synthesis method that combines soft lithography and self-assembly. By utilizing a patterned template with controlled wettability, precise manipulation of LHP crystal formation is achieved, enabling the fabrication of patterned LHP structures with high crystalline quality. This innovative approach offers a scalable and practical pathway for incorporating LHPs into advanced photonic devices. This thesis will comprehensively explore LHPs, characterizing their structures, investigating their potential, and validating a novel patterning method. This comprehensive analysis aims to advance the understanding and utilization of LHPs, paving the way for their integration into next-generation photonic devices.

Acknowledgment

I would like to express my deepest gratitude to my supervisor, Dr. Yanan (Laura) Wang, for her invaluable guidance, continuous support, and insightful feedback throughout the course of this research. Her expertise and dedication have been instrumental in the successful completion of this thesis. I am profoundly grateful for the opportunities she provided me, which have greatly enriched my academic and research experience. I am also deeply thankful to my supervisory committee members, Dr. Yongfeng Lu and Dr. Yinsheng Guo, for their constructive feedback, encouragement, and valuable suggestions that have significantly contributed to the depth and quality of my research. A special thank you to my colleagues, Sanchaya Pandit and Dr. Ji Wang, for their constant support, encouragement, and collaborative spirit. Their contributions and shared insights have been pivotal in navigating the challenges of this research. I would also like to acknowledge the Department of ECE for providing the resources and support necessary for my research. A heartfelt thanks to the Nebraska Center for Materials and Nanoscience (NCMN) facility for their state-of-the-art equipment and technical assistance, which were crucial for the experimental aspects of this work.

Finally, I wish to extend my deepest appreciation to my family and friends for their unwavering support and encouragement throughout this journey. Their love, patience, and belief in me have been my driving force.

Contents

Chapter 1: Introduction

Background and Significance

Lead halide perovskites (LHPs) have garnered considerable attention in recent years due to their extraordinary potential in the realm of photonic materials. [1] These materials, which include the three-dimensional (3D) $APbX_3$ phase, the two-dimensional (2D) APb_2X_5 phase, and the zero-dimensional (0D) A_4PbX_6 phase, exhibit a wide range of structural configurations with "A" representing a monovalent cation (such as Cs^+ or MA^+) and "X" representing a halide anion (such as Cl^-, Br^-, or I^-). This structural diversity contributes to their highly tunable photophysical properties, making LHPs highly attractive for applications in photovoltaics and optoelectronics.[2] Additionally, the ease of synthesis via hydrothermal reactions adds to their appeal for both research and industrial applications.

However, harnessing the full potential of LHPs is not without its challenges. The complex phase equilibrium and chemical inherent to LHPs pose significant obstacles, particularly when it comes to patterning these materials into sophisticated photonic structures using traditional lithography and etching techniques. These conventional methods often fall short, as they can lead to material degradation and a loss of crystallographic integrity, thereby compromising the performance of the final devices.

In response to these challenges, this thesis proposes an innovative synthesis method that combines soft lithography with self-assembly. This novel approach utilizes a patterned template with asymmetric wettability to precisely control nucleation and crystal growth.[3] The result is the formation of LHP structures with high crystallographic order, which is crucial for achieving optimal performance in optoelectronic devices. By leveraging this method, it becomes possible to create highly ordered perovskite structures in a scalable and feasible manner, paving the way for the development of integrated photonic devices based on LHPs.

The significance of this research lies not only in addressing the current limitations of LHP fabrication but also in opening new avenues for their application. By enhancing our understanding of the structural characteristics and synthesis methods of LHPs, this work aims to contribute to the broader field of materials science and optoelectronics, driving forward the development of next-generation photonic devices.

Overview of Lead Halide Perovskites

Lead halide perovskites (LHPs) are characterized by their diverse crystalline structures and remarkable optoelectronic properties. The three-dimensional (3D) structure, denoted as $APbX_3$, consists of a network of corner-sharing PbX_6 octahedra with A cations occupying the interstitial sites. The two-dimensional (2D) APb_2Br_5 phase features layers of PbX_6 octahedra separated by A cations (Cs^+), while the zero-dimensional (0D) A_4PbX_6 phase comprises isolated PbX_6 octahedra within a matrix of A cations as seen in figure 1.1. These varying structures offer unique advantages for different applications, particularly in the field of photonics.

The exceptional excitonic transitions in LHPs arise from their unique crystal structures, which enable strong light-matter interactions. Furthermore, the tunability of their photophysical properties allows for precise control over their optical and electronic behaviors, making them ideal candidates for a wide range of optoelectronic applications, including solar cells, LEDs (Light-Emitting Diode), and photodetectors.

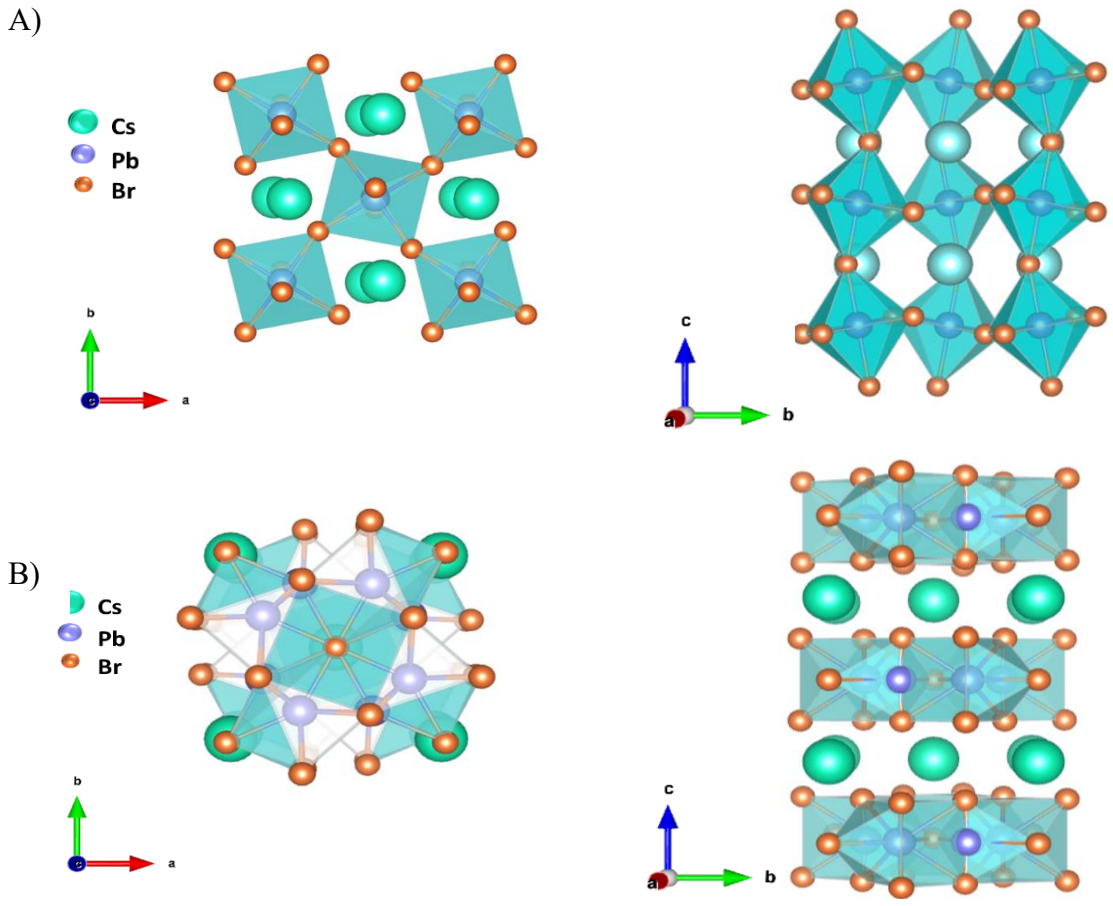

Figure 1.1: A) Crystal structure of $CsPbBr_3$ B) Crystal structure of layered $CsPb_2Br_5$ perovskite: $[Pb_2Br_5]^{4-}$ polyhedron separated by Cs^+ ions.

Historical Context and Development of Perovskites

The discovery and evolution of perovskite materials have a rich historical context. The term "perovskite" was first coined in 1839 by Gustav Rose for the mineral $CaTiO_3$, named after Count Lev Alekseyevich von Perovski. In 1926, Victor Goldschmidt expanded the term to describe a broader class of materials with similar crystal structures. [4] Naturally occurring perovskites are predominantly oxides, but synthetic perovskites have expanded this definition to include a wide range of compositions, including lead halide perovskites.

The advent of LHPs has revolutionized materials science, particularly in the fields of photovoltaics and optoelectronics. The flexibility of the perovskite structure allows for the accommodation of various elements and the formation of complex compounds, leading to significant advancements and new opportunities in material design and application.

Types of Lead Halide Perovskites

Perovskites can be broadly categorized based on their dimensionality, composition, and structural properties. The primary types of perovskites relevant to this thesis include:

Three-Dimensional (3D) Perovskites ($APbX_3$): These perovskites have a three-dimensional framework of corner-sharing BX_6 octahedra with A cations occupying the interstitial spaces. This structure provides a unique combination of high charge-carrier mobility and strong light absorption, making them suitable for high-efficiency solar cells and LEDs.

Two-Dimensional (2D) Perovskites (APb_2X_5): In these perovskites, layers of PbX_6 octahedra are separated by A cations. The layered structure offers enhanced stability against moisture and other environmental factors. However, the reduced dimensionality can lead to different electronic properties, such as lower charge-carrier mobility and increased exciton binding energy, compared to their 3D counterparts.

Zero-Dimensional (0D) Perovskites (A_4PbX_6): These perovskites consist of isolated PbX_6 octahedra within a matrix of A cations The discrete nature of the octahedra confines excitons within individual octahedra, leading to unique optical properties such as narrow emission spectra. The lack of interaction between neighboring octahedra results in sharp and well-defined emission peaks. However, while this property is advantageous for certain applications such as lighting and displays, it might not be ideal for all LED applications. For LEDs, materials that offer a broader range of tunable emissions and higher charge-carrier mobility are often preferred.

Mixed-Cation and Mixed-Halide Perovskites: By incorporating different cations (e.g., Cs, MA, FA) or halides (e.g., I, Br, Cl), researchers can fine-tune the properties of

perovskites to achieve desired performance metrics for specific applications. This approach allows for the optimization of bandgaps, stability, and overall device efficiency.

Understanding the phase stability and transformation pathways of $CsPbBr_3$ is crucial for optimizing their performance and stability in these applications. The stability of perovskite phases is influenced by the chemical environment, specifically the relative concentrations of cesium (Cs) and lead (Pb), as well as the presence of solvents (Zhou et al.). In a balanced stoichiometric environment, $CsPbBr_3$ primarily exists in a cubic phase, which is characterized by its highly symmetric crystal structure. However, the chemical environment can shift this balance, leading to different perovskite phases. Under Pb-rich conditions, $CsPbBr_3$ can transform into $CsPb_2Br_5$, a phase where the ratio of Pb to Cs increases. This transformation occurs through the loss of CsBr, a compound that is less stable in a Pb-rich environment. Conversely, in a Cs-rich environment, the excess Cs leads to the formation of Cs_4PbBr_6, where the ratio of Cs to Pb is higher. This transformation is facilitated by the addition of CsBr.

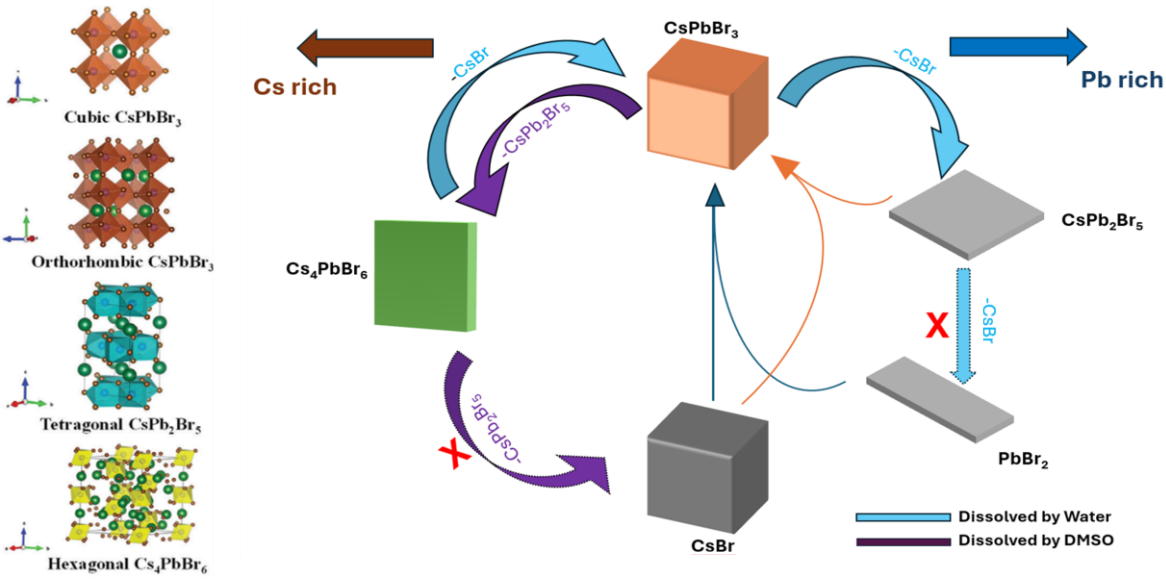

Figure 1.2: Transformation pathways among various cesium lead bromide $CsPbBr_3$ perovskite structures, illustrating the impact of Cs-rich and Pb-rich environments on phase stability. The figure shows transitions between $CsPbBr_3$, $CsPb_2Br_5$, and Cs_4PbBr_6, highlighting the role of CsBr addition and removal. Solvent effects are also depicted, water dissolving $CsPbBr_3$ (blue arrows) and DMSO dissolving $CsPb_2Br_5$ (purple arrows). Certain transformations are restricted, as indicated by red 'X' marks, demonstrating non-feasible pathways. Adapted from Zhou et al [15].

Solvents also play a significant role in these phase transitions. For example, $CsPbBr_3$ is more soluble in water, which can drive the dissolution and phase transformation processes to $CsPb_2Br_5$. On the other hand, when $CsPbBr_3$ dissolves in DMSO (dimethyl

sulfoxide), a common solvent used in perovskite synthesis and processing, the phase transformation to Cs_4PbBr_6 occurs. [15]

Figure 1.2 demonstrates these phase transformations and the impact of chemical environments and solvents on the stability of $CsPbBr_3$. It highlights the main transformation pathways between different phases: $CsPbBr_3$, $CsPb_2Br_5$, and Cs_4PbBr_6.

The controllable phase transition between $CsPb_2Br_5$ and $CsPbBr_3$ is crucial for optimizing photonic and optoelectronic devices, achieved through various mechanisms such as thermal treatment, chemical modification, solvent engineering, mechanical pressure, and notably, laser irradiation.

Thermal treatment involves heating $CsPb_2Br_5$ to a temperature that induces its decomposition into $CsPbBr_3$ and $PbBr_2$. [16] The thermal energy disrupts the crystal lattice, allowing bromide ions to rearrange into the more stable $CsPbBr_3$ phase at 250^0C to 300^0C.

Chemical environment modification, such as introducing additional bromide ions or lead ions, drives the transition between phases by altering the chemical potential. An excess of bromide ions facilitates the reorganization of the crystal structure into $CsPbBr_3$, while the removal of bromide or the addition of a stabilizing agent promotes the formation of $CsPb_2Br_5$. [17] This method allows precise control over the phase through chemical stoichiometry.

Solvent engineering utilizes polar solvents to selectively dissolve and recrystallize the perovskite phases. The solvation energy from polar solvents breaks the ionic bonds in $CsPbBr_3$, leading to its dissolution. Upon controlled solvent evaporation, $CsPb_2Br_5$ can nucleate and grow, allowing for phase transition through solution processing. [18] This approach manipulates the material's phase at room temperature and ambient pressure.

Among these methods, laser irradiation stands out for its precision and control. When $CsPb_2Br_5$, absorbs laser photons, localized heating occurs, generating high-energy states within the crystal lattice. [19] This localized energy input breaks bonds and facilitates atomic rearrangement, promoting the transition to $CsPbBr_3$. Laser irradiation allows for highly localized phase transitions, enabling precise patterning and structuring of the material on a micro- to nanoscale. Non-thermal effects, such as photon-induced ionization and excitation of electronic states, further drive the phase transition by altering the chemical potential and promoting ion mobility.

Using laser irradiation to manipulate the phase transition is particularly advantageous because it delivers controlled, localized energy that precisely affects the material's phase without impacting surrounding areas. This non-contact method reduces the risk of contamination and mechanical damage, making it ideal for delicate perovskite structures. Additionally, the tunable parameters of the laser, such as intensity, wavelength, and

duration, provide fine-tuned control over the phase transition process, enabling the creation of complex and functional patterns.

By understanding and leveraging these phase transition mechanisms, especially the benefits of laser irradiation, researchers can precisely tune material properties. This enhances the performance and stability of perovskite-based devices, making them highly efficient for applications in LEDs, solar cells, and photodetectors. These advancements pave the way for developing advanced perovskite technologies with superior functionality and new capabilities.

.

Photonic Applications of Lead Halide Perovskite

Lead halide perovskites have garnered significant attention in photonics research due to their exceptional optoelectronic properties. These materials exhibit tunable bandgaps typically ranging from approximately 1.2 to 3.0 eV and can achieve high photoluminescence quantum efficiencies, often exceeding 90% in optimized conditions. making them ideal for a variety of photonic applications, including photovoltaics, light-emitting diodes (LEDs), lasers, and sensors.[6]

One of the key advantages of lead halide perovskites is their tunable bandgap, which can be adjusted by modifying the halide composition. This tunability allows for the optimization of perovskite materials for specific photonics applications. For instance, $CsPbBr_3$ has a bandgap of approximately 2.4 eV, making it suitable for green emission, while $CsPbI_3$ with a bandgap of around 1.73 eV is more appropriate for applications in the near-infrared region. This flexibility is a crucial factor in their widespread use in optoelectronic devices.

The unique band structures of $CsPbBr_3$ and $CsPb_2Br_5$ open up numerous possibilities for advanced photonic applications. $CsPbBr_3$ exhibits a direct bandgap of approximately 2.4 eV, with the conduction band primarily composed of lead (Pb) 6p orbitals and the valence band consisting mainly of bromine (Br) p orbitals. This band structure enables efficient electron transport and effective light absorption, making $CsPbBr_3$ suitable for various optoelectronic applications. With its direct bandgap, $CsPbBr_3$ is particularly well-suited for light-emitting diodes (LEDs). Its high photoluminescence quantum yield allows for efficient light emission, making it ideal for devices that operate in the green to blue spectrum. This material's ability to absorb visible light efficiently also makes it an excellent candidate for photodetectors, where its rapid photoresponse and high sensitivity are highly valued.

In contrast, $CsPb_2Br_5$ is characterized by a larger bandgap of 3.58 eV, indicating its suitability as a dielectric material. Similar to $CsPbBr_3$, its conduction band is derived from lead (Pb) 6p orbitals, and the valence band from bromine (Br) p orbitals. The large

bandgap positions $CsPb_2Br_5$ as an ideal candidate for applications requiring high breakdown voltages and stability under extreme conditions. This wide bandgap enables the detection of high-energy UV photons with minimal noise, providing high selectivity and reliability.[7] Moreover, the stability and broad bandgap of $CsPb_2Br_5$ make it a prime material for UV laser diodes, which are crucial for applications that require precise and powerful UV light sources.

In terms of light emission, lead halide perovskites exhibit outstanding performance due to their high photoluminescence quantum yield (PLQY) and significant excitonic effects at room temperature. $CsPbBr_3$, for example, is considered a viable alternative to InGaN for green LEDs because of its similar bandgap and superior defect tolerance. This addresses the green-gap problem, a major challenge in the development of efficient green LEDs. The high PLQY of these materials also benefits applications in lasers and displays, where bright and efficient light emission is essential.[8]

The ability of lead halide perovskites to form various nanostructures further enhances their applicability in photonics. Nanostructures such as quantum dots, nanowires, and nanoplates each offer unique advantages. Quantum dots can efficiently confine light, enhancing light-matter interaction and improving light emission. Nanowires can serve as Fabry–Pérot microresonators, guiding light along their axis with high cavity quality factors, which is advantageous for laser applications. Nanoplates can support whispering gallery modes, contributing to efficient lasing.[9]

Figure 1.3 displays the Density Functional Theory (DFT) calculated electronic band structures for various cesium lead bromide perovskite phases, illustrating their unique electronic properties. The top left panel shows cubic $CsPbBr_3$, which has a direct bandgap at the Gamma (Γ) point, beneficial for optoelectronic applications like solar cells and LEDs due to its efficient light absorption and emission. The orthorhombic $CsPbBr_3$ phase, shown in the top right panel, also has direct electronic transitions, though its complex band arrangement differs from the cubic phase, still supporting strong optical properties. The bottom left panel presents $CsPb_2Br_5$, characterized by an indirect bandgap, resulting in lower photoluminescence efficiency but offering high stability for specific applications. Lastly, the bottom right panel illustrates Cs_4PbBr_6, with a wider bandgap and minimal band dispersion, known for its narrow emission spectra, suitable for display and lighting applications

Integration of lead halide perovskites into hybrid structures has become a significant research focus. Combining these perovskites with established materials such as silicon in photonic devices can leverage the strengths of both materials, leading to enhanced performance and new functionalities. Hybrid structures can improve light absorption, reduce reflection losses, and enable novel applications such as metasurfaces and meta optics. Metasurfaces made from lead halide perovskites can manipulate light at

subwavelength scales, offering new possibilities for dynamic color displays and broadband antireflective coatings

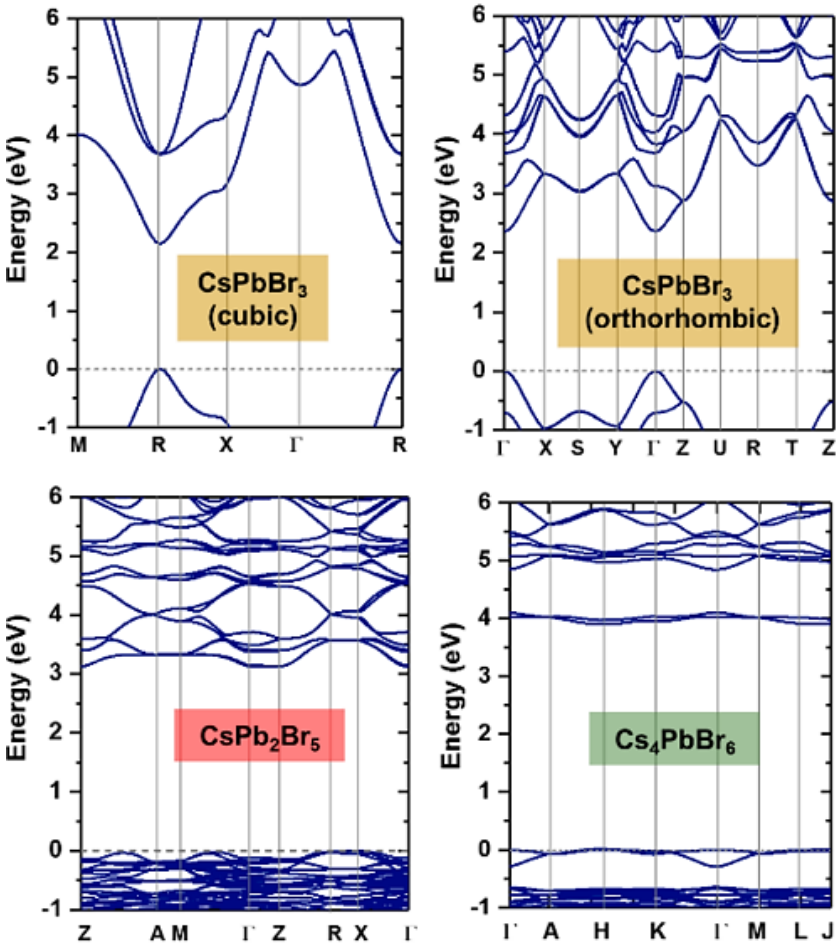

Figure 1.3: The Density Functional Theory (DFT) calculated electronic band structures of various cesium lead bromide perovskite phases. The top left panel shows the band structure of cubic $CsPbBr_3$, the top right panel displays the orthorhombic $CsPbBr_3$ phase, the bottom left panel illustrates the band structure of $CsPb_2Br_5$, and the bottom right panel depicts Cs_4PbBr_6. [14]

Lead halide perovskites also exhibit promising nonlinear optical properties. Despite their centrosymmetric crystal structure, which typically suppresses second harmonic generation (SHG), these materials demonstrate SHG due to ferroelectric domains.[10] This nonlinearity opens up new avenues for applications in ultrafast optics and photonic devices operating on at-second timescales. High-harmonic generation in lead halide perovskites has been demonstrated, underscoring their potential for generating broadband light sources and exploring new regimes of nonlinear optics.

Advantages of Perovskites as Photonic Material Platforms Compared to Traditional Materials

Perovskites offer distinct advantages over traditional photonic materials like silicon (Si), silicon nitride (Si_3N_4), and gallium nitride (GaN), particularly in tunability and processing flexibility. Unlike silicon's indirect bandgap, $CsPbX_3$ has a tunable direct bandgap, allowing precise control over optical properties and making them versatile for various photonic applications, from visible to near-infrared wavelengths. Moreover, the narrow bandgap of silicon (1.1 eV) results in significant absorption over the entire visible spectrum, thus limiting its application in visible photonic cavities or waveguiding devices.

Silicon nitride (Si_3N_4) is valued for its high thermal stability and compatibility with existing silicon processing infrastructure, making it a staple in photonic integrated circuits due to its low propagation loss. However, Si_3N_4 lacks the tunability and light-emission efficiency of perovskites. Perovskites' ability to be processed from solution at low temperatures enables cost-effective and scalable fabrication methods such as spin-coating, inkjet printing, and roll-to-roll processing, which are simpler and more versatile compared to the high-temperature and high-vacuum deposition techniques required for Si_3N_4.

Gallium nitride (GaN) is renowned for its high efficiency and stability, particularly in high-power electronic devices and LEDs, thanks to its direct wide bandgap. However, GaN devices typically necessitate high-temperature growth processes, which are both costly and complex. Moreover, GaN is less defect-tolerant compared to perovskites, requiring high-quality substrates and meticulous epitaxial growth techniques. In contrast, perovskites demonstrate remarkable tolerance to defects, maintaining their optoelectronic properties even with imperfections in the crystal structure, which significantly simplifies their fabrication requirements.

Also, as discussed above, the phases of perovskite can be easily controlled, offering diverse band structures and optical properties from wide bandgap to luminant phases. It can be envisioned that a monolithic platform can be developed with wide-bandgap $CsPb_2Br_5$ as cavity and semiconducting $CsPbBr_3$ as emitter to form a unique cavity-emitter coupled platform for exploring quantum photonic phenomena.

Another critical advantage of perovskites over these mature platforms is their compatibility with flexible substrates. The low-temperature, solution-based processing of perovskites allows for their deposition on flexible materials, paving the way for the development of flexible and wearable photonic devices. This flexibility is challenging to achieve with rigid materials like silicon and GaN, further highlighting the unique potential of perovskites in advancing photonic technologies.

Chapter 2: Methodology and Characterization

Solvothermal Synthesis of Cesium Lead Bromide Perovskites

Solvothermal synthesis is a widely used method for producing high-quality lead halide perovskites (LHPs) due to its precise control over the crystal growth environment. In our study, we employed a solvothermal approach to synthesize cesium lead bromide perovskites ($CsPbBr_3$) using cesium bromide (CsBr) and lead bromide ($PbBr_2$) as precursors dissolved in either hydrobromic acid (HBr) or dimethyl sulfoxide (DMSO).

The primary difference between these two methods lies in the role and effect of HBr and DMSO in the synthesis process. Using HBr directly supplies bromide ions and improves stoichiometric control, potentially leading to higher purity and crystallinity in the final perovskite films. In contrast, DMSO, as a coordinating solvent, provides better control over the nucleation and growth of crystals, resulting in films with larger grain sizes and enhanced uniformity.

Both methods have unique advantages, and the choice between them can depend on the specific requirements of the intended application. For instance, if high crystallinity and purity are paramount, the HBr method might be preferred. Conversely, if larger grain sizes and improved film uniformity are desired, the DMSO method could be more suitable.

Fume Hood and Chemical Bench

The primary principle of a fume hood is containment. It is designed to enclose hazardous fumes, vapors, and dust to protect the user from exposure to harmful substances. The second principle is air flow. The fume hood operates by drawing air from the laboratory and expelling it outside, creating a negative pressure environment inside the hood. This ensures that contaminants are directed away from the user, reducing the risk of inhalation or contact. Some fume hoods also incorporate filtration systems as a third principle. These systems capture harmful particles and vapors before the air is released outside or recirculated back into the laboratory, providing an additional layer of protection.

A fume hood is an essential safety device in laboratories, designed to protect researchers from exposure to hazardous chemicals and substances. It typically consists of a ventilated enclosure with a sash window that can be adjusted to control the airflow and provide a barrier between the user and the harmful materials. The fume hood's exhaust system safely removes contaminated air from the lab, ensuring a safer working environment. Proper use and maintenance of fume hoods are crucial for effective protection and compliance with safety regulations. Regular inspections and adherence to operational guidelines ensure that the fume hood functions efficiently, safeguarding the health and

safety of laboratory personnel. By maintaining a controlled environment, fume hoods play a vital role in preventing accidents and minimizing the risk of chemical exposure in research and industrial settings.

Figure 2.1: A fume hood in a laboratory setting, equipped for safely handling and venting hazardous chemicals, ensuring a controlled environment for experiments involving flammable and acidic substances.

Raman Spectrometer (LabRAM HR Evolution by HORIBA Scientific)

The Raman spectrometer operates based on the principle of Raman scattering. When a sample is illuminated with a monochromatic light source, typically a laser, most of the light is scattered elastically (Rayleigh scattering). A small portion of the light, however, is scattered inelastically due to interactions with the molecular vibrations, rotations, and other low-frequency modes in the sample. This inelastic scattering is known as Raman scattering. The Raman spectrometer detects the frequency shift in the scattered light, which provides a molecular fingerprint unique to the sample.

The LabRAM HR Evolution Raman spectrometer by HORIBA Scientific is an advanced analytical instrument used to identify molecular composition and structure through Raman spectroscopy. It is equipped with a high-resolution monochromator, a sensitive CCD detector, and various laser sources to analyze different types of samples. This spectrometer can perform detailed chemical analysis by detecting the vibrational, rotational, and other low-frequency modes of molecules.

In the field of photonics, the LabRAM HR Evolution is particularly useful for studying photoluminescence (PL) spectra. Photoluminescence spectroscopy involves the absorption of photons by a material, followed by the emission of photons as the material returns to a lower energy state. By analyzing the PL spectra, researchers can gain insights into the electronic and optical properties of materials, such as bandgap energies, defect levels, and quantum efficiency.

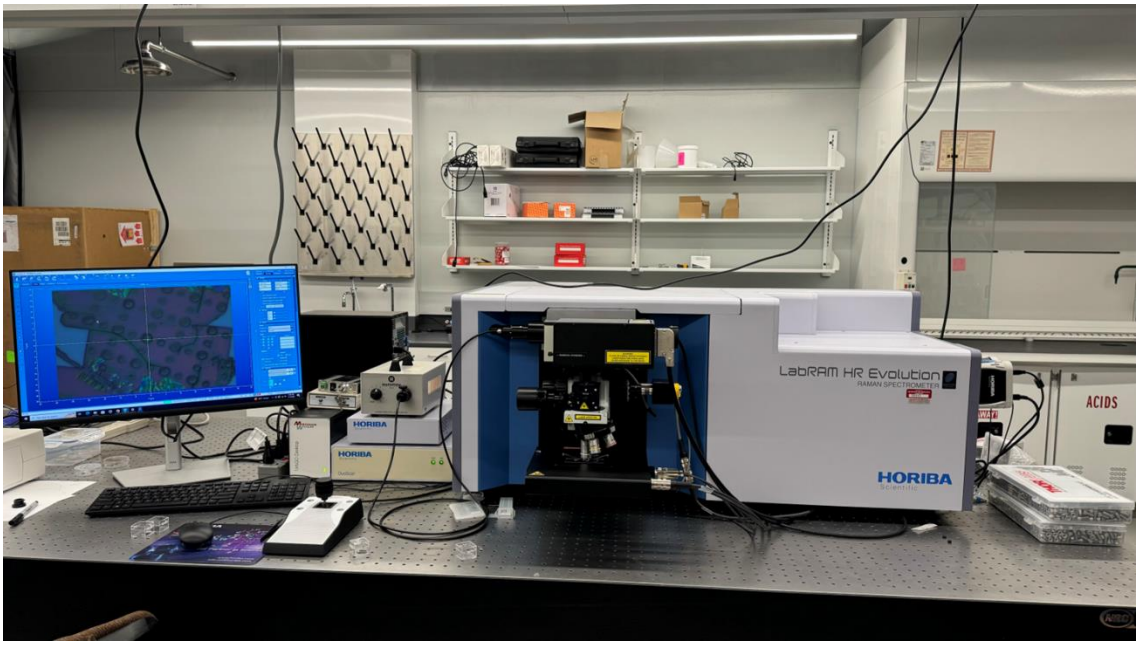

Figure 2.2: LabRAM HR Evolution Raman Spectrometer by HORIBA Scientific set up for photoluminescence (PL) spectroscopy analysis, providing detailed insights into the electronic and optical properties of photonic materials.

The LabRAM HR Evolution is well-suited for PL spectroscopy due to its high sensitivity and resolution, allowing for the detection of even weak photoluminescence signals. It is widely used in the development and characterization of photonic materials, including semiconductors, quantum dots, and light-emitting materials. The ability to combine Raman and PL measurements in a single instrument provides a comprehensive tool for materials research, enabling detailed analysis of both vibrational and electronic properties.

The device is user-friendly with sophisticated software that allows for detailed data acquisition and analysis. Regular calibration and maintenance are crucial to ensure the accuracy and reliability of the measurements obtained from the Raman spectrometer. By providing critical insights into the optical properties of materials, the LabRAM HR Evolution plays a vital role in advancing photonic applications and technologies.

Heidelberg DWL 66FS Laser Lithography System

The Heidelberg DWL 66FS operates based on the principles of laser lithography. Laser lithography uses a focused laser beam to transfer a geometric pattern from a digital file onto a substrate coated with a photosensitive material (photoresist). The laser beam directly writes the pattern by selectively exposing the photoresist, which then undergoes chemical changes in the exposed areas. These changes allow for subsequent development processes to create the desired micro- or nanostructures on the substrate.

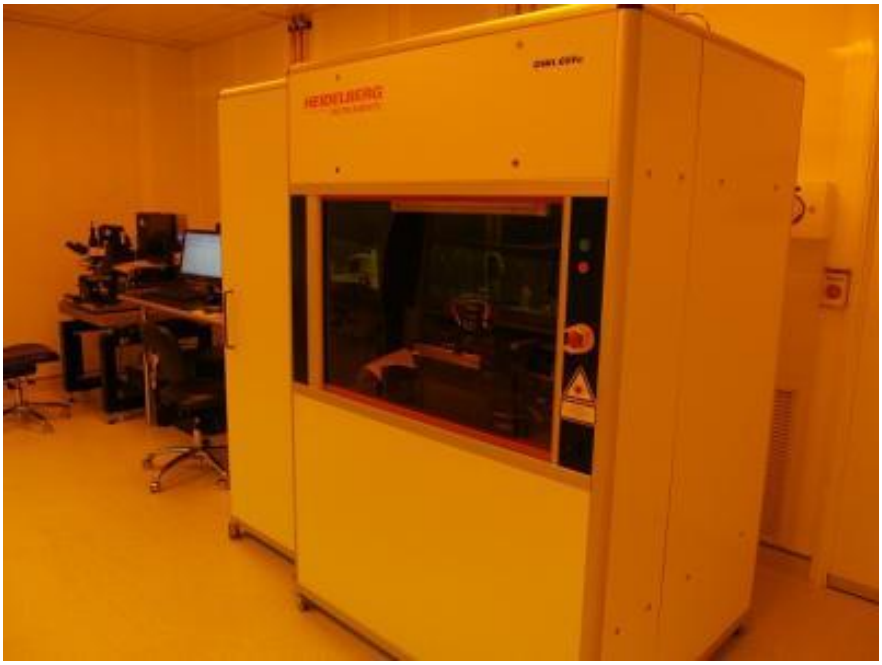

Figure 2.3: Heidelberg DWL 66FS Laser Lithography System in a cleanroom environment, used for creating high-precision micro- and nanostructures essential for advanced photonic applications and microfabrication.

The Heidelberg DWL 66FS Laser Lithography System is a high-precision tool used for creating intricate patterns and structures on various substrates, essential for applications in microfabrication and nanotechnology. This system is highly versatile, allowing for the fabrication of photonic devices, micro-optical elements, and other advanced materials. It

is capable of producing features down to the sub-micron scale with high accuracy and repeatability.

In photonics, the DWL 66FS is particularly valuable for fabricating photonic crystals, waveguides, and other components that require precise control over feature sizes and shapes. The ability to directly write patterns without the need for masks accelerates the prototyping process and enhances flexibility in design iterations. The system is equipped with advanced software for layout design, exposure control, and alignment, ensuring that complex patterns can be accurately and efficiently transferred onto the substrate.

Regular calibration and maintenance are necessary to maintain the precision and performance of the laser lithography system. By enabling the production of high-resolution patterns, the Heidelberg DWL 66FS plays a crucial role in the development and manufacturing of cutting-edge photonic and microelectronic devices

Oxford PlasmaPro 100 Deep RIE System

The Oxford PlasmaPro 100 Deep Reactive Ion Etching (RIE) system operates based on the principle of plasma-assisted etching. In this process, a plasma is generated by applying a high-frequency electric field to a low-pressure gas, creating a mixture of ions, electrons, and neutral particles. The reactive ions in the plasma bombard the substrate, etching away material in a highly controlled manner. Deep RIE is specifically designed to achieve high aspect ratio structures, where the depth of the etch is much greater than the width. This is accomplished by alternating between etching and passivation steps, allowing for precise vertical sidewalls.

The Oxford PlasmaPro 100 Deep RIE System is an advanced tool used in the fabrication of micro- and nanostructures, particularly in semiconductor manufacturing and photonic applications. It is capable of producing highly precise and intricate patterns on a variety of materials, including silicon, III-V compounds, and dielectrics. This system is essential for creating features such as trenches, vias, and other high aspect ratio structures that are critical in the development of microelectromechanical systems (MEMS), integrated circuits, and photonic devices.

In photonic applications, the PlasmaPro 100 Deep RIE System enables the fabrication of optical waveguides, photonic crystals, and other components that require precise control over the etching process to achieve desired optical properties. The system's advanced process control, combined with its ability to handle complex etching recipes, ensures high repeatability and uniformity across the substrate.

Figure 2.4: Oxford PlasmaPro 100 Deep RIE System in a cleanroom environment, used for precise etching of semiconductor materials.

Regular calibration and maintenance are vital to ensure the optimal performance of the Deep RIE system. By providing high-precision etching capabilities, the Oxford PlasmaPro 100 Deep RIE System plays a crucial role in advancing the fabrication of next-generation photonic and electronic devices.

Rigaku SmartLab Diffractometer

The Rigaku SmartLab Diffractometer operates on the principle of X-ray diffraction (XRD). When a crystalline material is irradiated with X-rays, the incident rays are scattered by the crystal lattice. This scattering produces constructive interference at specific angles, known as Bragg angles, according to Bragg's law. The diffractometer measures the angles and intensities of these diffracted X-rays, providing information about the crystal structure, phase composition, and other material properties.

The Rigaku SmartLab Diffractometer is a sophisticated instrument used for analyzing the crystallographic structure of materials. It is equipped with a high-resolution X-ray source, advanced detectors, and a goniometer that precisely positions the sample. The SmartLab

system is highly versatile and can be configured for various XRD techniques, including powder diffraction, thin-film analysis, and small-angle X-ray scattering.

Figure 2.5: Rigaku SmartLab Diffractometer in a laboratory setting, used for detailed crystallographic analysis of materials

In photonics and materials science, the SmartLab Diffractometer is invaluable for characterizing the crystalline phases and orientations of materials used in optical and electronic devices. It can identify and quantify different phases, determine lattice parameters, and analyze the quality and thickness of thin films. The data obtained from XRD analysis are critical for understanding the material properties that influence the performance of photonic devices.

The Rigaku SmartLab Diffractometer features user-friendly software for data acquisition and analysis, making it accessible for both novice and experienced researchers. Regular calibration and maintenance are essential to ensure the accuracy and reliability of the measurements. By providing detailed insights into the structural properties of materials, the Rigaku SmartLab Diffractometer plays a crucial role in advancing research and development in various scientific and industrial fields.

Chapter 3: Optimization of Bulk Crystal Synthesis

The optimization and synthesis of bulk cesium lead bromide ($CsPbBr_3$ and $CsPb_2Br_5$) crystals were conducted using a controlled solvothermal method. The precursors used in this synthesis were cesium bromide (CsBr) and lead bromide ($PbBr_2$), with hydrogen bromide (HBr) serving as a critical reactant to enhance the crystal quality and purity.

Synthesis Protocol

The synthesis of $CsPb_2Br_5$ crystals was carried out following the method described by Zhang, Zhaojun, et al. This method involved meticulous preparation of precursor solutions and controlled deposition to achieve high-quality crystals.[11]

We measured 0.3 mmol of CsBr powder (0.06 g, Sigma, 99%) and dissolved it in 2 mL deionized HBr (48% aq., Sigma) to obtain the Cs-solution. Separately, 0.6 mmol of PbBr2 (0.22 g, Aladdin, 99%) powder was dissolved in 3 mL HBr (48% aq., Sigma) to obtain the Pb-solution. Both solutions were kept heated at 90 ℃. The Cs-solution was then added dropwise into the Pb-solution under vigorous stirring, resulting in a clear solution.

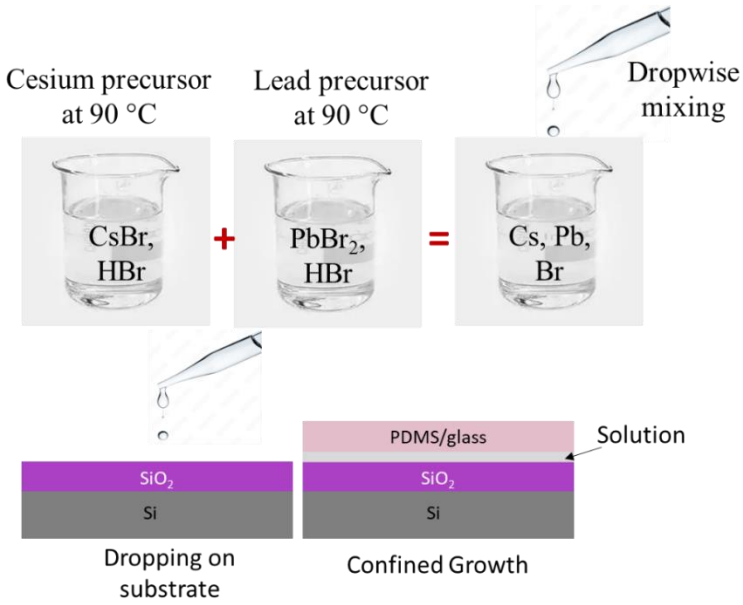

Figure 3.1: Synthesis Process of $CsPb_2Br_5$ and $CsPbBr_3$ Nanowires Schematic showing the synthesis of $CsPb_2Br_5$ crystals and $CsPbBr_3$ nanowires. CsBr and PbBr2 are dissolved in HBr, mixed, and either cooled slowly or drop-casted on substrates for crystal formation.

The solution was slowly cooled from 90 ℃ to room temperature. Within 0.5 hours, small-area colorful $CsPb_2Br_5$ crystals were obtained. By maintaining a slow cooling rate of

approximately 5 °C/h, large-area transparent flake crystals, up to 5×5 mm^2 in size, were obtained after 2.5 hours.

Alternatively, the solution was drop-casted onto SiO_2/Si substrates and covered with a glass or PDMS layer to ensure confined growth. This method promoted the formation of large $CsPbBr_3$ nanowires. The controlled environment facilitated the growth of elongated nanowires with uniform dimensions, suitable for various applications.

Controlling nucleation in hydrothermal synthesis to achieve large-size single crystals of perovskites requires precise management of several parameters. A specific protocol involving the gradual addition of a heated CsBr solution into a heated $PbBr_2$ solution at 90°C has been developed to optimize this process. By maintaining both solutions at the same temperature, the protocol ensures uniform thermal conditions that prevent sudden temperature gradients and enhance the solubility of precursor materials. This controlled environment helps achieve a supersaturated solution conducive to nucleation once the solutions are mixed. The gradual addition of CsBr into $PbBr_2$ promotes homogeneous mixing and controlled supersaturation. This method prevents rapid nucleation and encourages the growth of fewer, larger crystals. Uniform nucleation throughout the solution is essential for producing high-quality, large-size single crystals. The controlled mixing also manages the supersaturation level, balancing nucleation and growth processes to maintain stability and prevent premature precipitation. Consistent pressure helps maintain steady growth conditions, while pure solvents with minimal impurities ensure consistent and controlled growth. Seed crystals provide predetermined nucleation sites, reducing random nucleation events and fostering the development of larger crystals. Extending the growth duration under stable conditions and utilizing specific additives or mineralizers can promote crystal growth over new nucleation, enhancing crystal size and quality. Controlled cooling after the growth phase allows existing crystals to grow larger without additional nucleation.[20]

If the protocol is reversed, with $PbBr_2$ being dropped into CsBr, the nucleation and crystal growth dynamics can change, potentially affecting the crystal quality and size. The reversed protocol may lead to rapid local supersaturation and numerous small nucleation sites, resulting in smaller and less uniform crystals. Poor mixing and localized high concentrations of Pb^{2+} ions can cause uneven nucleation and growth, leading to crystals of varying sizes and qualities. The potential temperature gradients and slower reaction kinetics may also introduce more defects into the crystals, reducing their optical and electronic properties.

Results and Characterization

The synthesized $CsPb_2Br_5$ crystals and $CsPbBr_3$ nanowires underwent comprehensive characterization to confirm their structural and optical properties. Optical microscopy

images revealed uniform and well-defined morphologies, with crystal dimensions ranging from micrometers to millimeters.

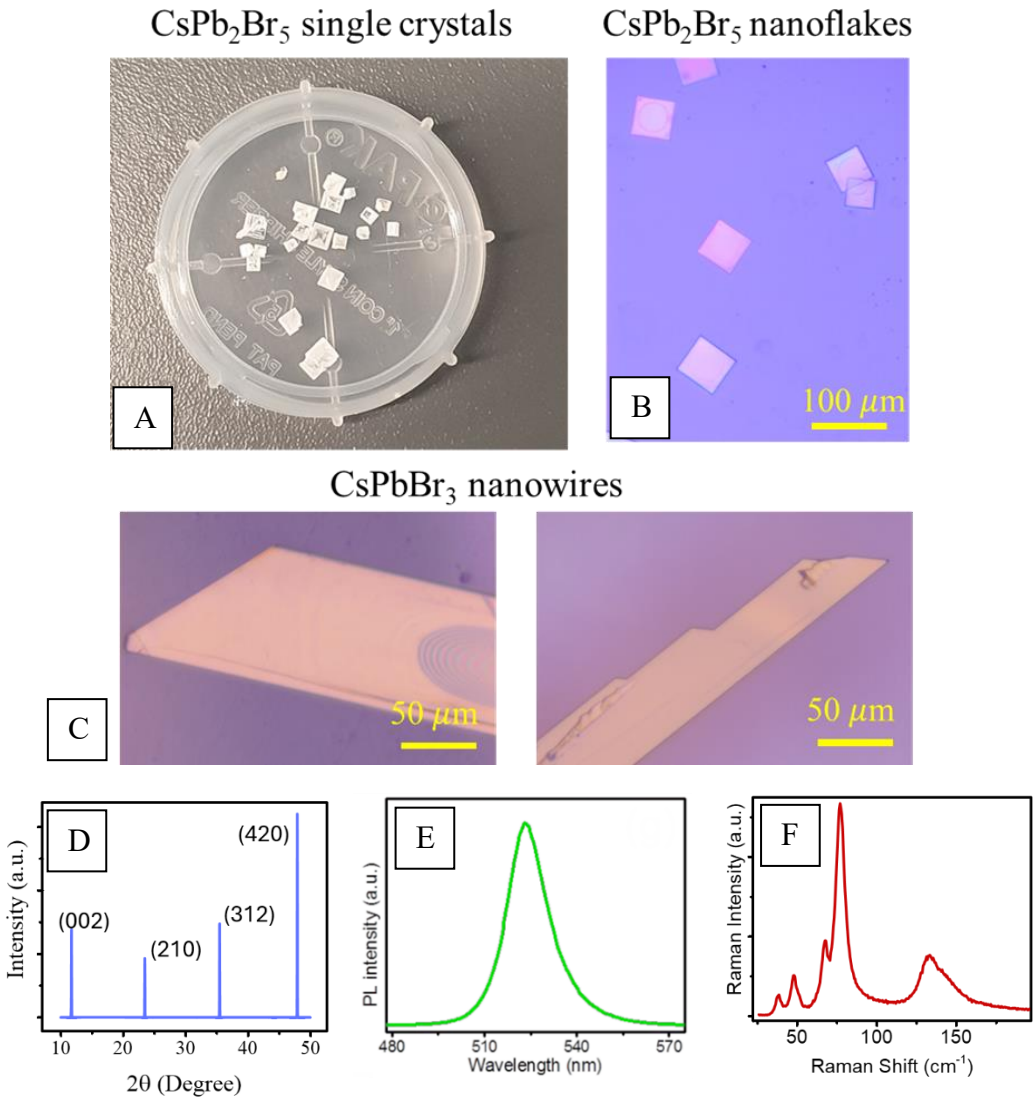

.

Figure 3.2: Characterization of CsPb2Br5 Crystals and CsPbBr3 Nanowires (A) Optical image of CsPb2Br5 crystals with well-defined cuboid morphology, demonstrating successful synthesis. (B) High magnification images of CsPb2Br5 crystals, showing uniform and precise cubic shapes. (C) High magnification images of CsPbBr3 nanowires, illustrating their elongated structure and uniform dimensions. (D) XRD spectrum with distinct peaks indicating high crystallinity and phase purity of CsPb2Br5 crystals. (E) PL spectrum showing a sharp emission peak at 525 nm, indicating excellent optical quality for optoelectronic applications. (F) Raman spectrum highlighting the vibrational modes, confirming the structural integrity of the synthesized materials

X-ray diffraction (XRD) analysis confirmed the crystallinity and phase purity of the $CsPb_2Br_5$ crystals. The XRD patterns showed distinct peaks corresponding to $CsPb_2Br_5$

crystal planes, indicating high crystallinity and successful synthesis. The XRD spectrum matched well with expected diffraction peaks, underscoring the phase purity of the material.

Photoluminescence (PL) spectroscopy revealed a sharp emission peak at around 525 nm, characteristic of the Br_3 complex. This suggested excellent optical quality for both $CsPb_2Br_5$ crystals and $CsPbBr_3$ nanowires, indicating strong luminescence properties suitable for optoelectronic applications.

Raman spectroscopy provided insights into the vibrational modes of the crystal lattice. The Raman spectrum displayed prominent peaks corresponding to specific phonon modes, validating the structural integrity of the synthesized crystals.

In summary, the detailed characterization using optical microscopy, XRD, PL spectroscopy, and Raman spectroscopy confirmed the high structural and optical quality of $CsPb_2Br_5$ crystals and $CsPbBr_3$ nanowires. These findings highlight their potential for advanced optoelectronic applications.

Chapter 4: Development of Patterning Synthesis

Template Preparation for Lead Halide Perovskites

In this thesis, we developed a novel approach for fabricating templates used in the synthesis of lead halide perovskites (LHPs) by combining soft lithography with deep reactive ion etching (DRIE). This method leverages a patterned template with asymmetric wettability to control nucleation and crystal growth, enabling the creation of highly ordered LHP structures with excellent crystallographic properties.[12]

Process Overview

1. Spin Coating Photoresist: The process begins with a silicon (Si) substrate coated with a silicon dioxide (SiO_2) layer. The SiO_2-coated Si substrate is spin-coated with a layer of photoresist. This involves depositing a few drops of photoresist solution onto the center of the substrate, which is then rapidly spun at high speeds (typically 2000-4000 rpm) to create a uniform thin film. The thickness of this film is controlled by the spin speed and duration, and it serves as the foundation for subsequent patterning steps.

2. Photolithography and Developing: After spin coating, the photoresist-coated substrate undergoes photolithography. During this step, the substrate is exposed to ultraviolet (UV) light through a photomask that contains the desired pattern. The UV exposure alters the chemical structure of the exposed photoresist, making it either more or less soluble in the developer solution, depending on whether a positive or negative photoresist is used. Following exposure, the substrate is immersed in a developer solution that selectively removes either the exposed or unexposed photoresist, revealing the underlying pattern on the SiO_2 layer.

3. Pattern Creation: The resulting patterned photoresist on the substrate defines the areas where etching will occur. We created two types of templates in this study: micro-trench and micro-hole templates. Micro-trench templates feature narrow, elongated channels, while micro-hole templates consist of circular or polygonal depressions. These distinct patterns are designed to influence the nucleation and growth of perovskite crystals, promoting highly ordered structures.

4. Deep Reactive Ion Etching (DRIE): Next, the patterned substrate undergoes DRIE to etch into the SiO_2 and Si layers. DRIE is a highly anisotropic etching technique that provides deep, vertical sidewalls with high precision. In this step, the substrate is placed in an etching chamber, where reactive ions are generated in plasma and directed towards the substrate. These ions bombard the exposed SiO_2 and Si, selectively removing material according to the patterned photoresist. DRIE allows for precise control over the etch depth and profile, creating well-defined micro-trenches and micro-holes in the substrate.

5. Lift-Off: Following the DRIE process, the remaining photoresist is removed using a solvent or plasma cleaning process, leaving behind the etched pattern on the SiO_2/Si substrate. This step, known as lift-off, ensures that only the desired pattern remains on the substrate, free of any residual photoresist.

6. FAS Coating and PDMS Stamping: The etched substrate is then treated with heptadecafluorodecyltrimethoxysilane (FAS) to modify its surface properties. FAS forms a self-assembled monolayer on the substrate surface, creating a hydrophobic (lyophobic) top surface and maintaining hydrophilic (lyophilic) sidewalls. This asymmetric wettability is crucial for controlling the nucleation and growth of perovskite crystals.

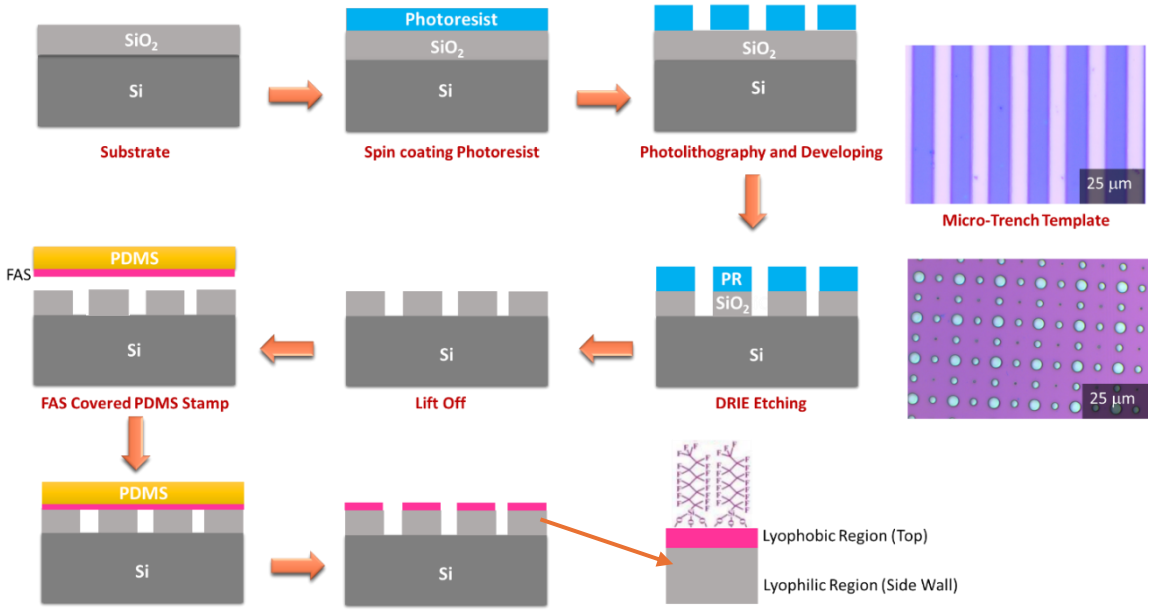

Figure 4.1: Schematic representation of the template fabrication process for lead halide perovskites using a combination of soft lithography and deep reactive ion etching (DRIE). The process includes spin coating a photoresist onto a SiO_2-coated Si substrate, patterning through photolithography and developing, etching via DRIE, and lifting off the remaining photoresist. The patterned substrate is then modified by stamping with a FAS-covered PDMS, resulting in templates with distinct lyophobic and lyophilic regions that guide perovskite crystal growth. Micrographs of the resulting micro-trench and micro-hole templates are shown on the right.

The FAS was kept in a vacuum chamber with polydimethylsiloxane (PDMS) to allow the FAS molecules to deposit onto the PDMS surface. Following this, the PDMS coated with FAS was stamped onto the patterned template for 3 minutes at 80°C. This process resulted in a modified template with distinct lyophobic (top) and lyophilic (sidewall) regions, which are essential for guiding the perovskite crystal growth during the synthesis process

The combination of soft lithography and deep reactive ion etching (DRIE) offers significant advantages for template fabrication in the synthesis of lead halide perovskites. This approach allows for high precision and control over the patterning process, enabling the creation of intricate and well-defined templates. The ability to create various patterns and structures provides flexibility to tailor the templates to specific applications, ultimately enhancing the performance and functionality of optoelectronic devices based on lead halide perovskites.

Patterning Synthesis of Lead Halide Perovskites

In this chapter, we discuss the patterning synthesis of lead halide perovskites (LHPs) using a modified micropillar structured template. The process leverages the asymmetric wettability of the template to control nucleation and crystal growth, resulting in highly ordered perovskite structures. The following steps outline the detailed procedure and principles behind the patterning synthesis.

A 0.3M precursor solution was prepared by dissolving stoichiometric amounts of CsBr and $PbBr_2$ in DMSO. The solution was then augmented with HBr to ensure the appropriate bromide ion concentration, enhancing the crystallinity and purity of the perovskite.

Patterning Synthesis Process:

1. **Dropping the Precursor Solution:** A 20 μL aliquot of the 0.3M precursor solution was carefully dropped onto the modified micropillar structured template. This template was designed with distinct lyophobic (top) and lyophilic (sidewall) regions to facilitate controlled crystal growth through capillary effects.
2. **Covering with Glass/Silicon:** After depositing the precursor solution, the template was covered with a glass or silicon substrate. This setup created a confined environment for the precursor solution within the micropillar structures.
3. **Evaporation and Crystal Growth:** The assembly was maintained at 60°C for 24 hours to allow for solvent evaporation. The asymmetric wettability of the template, resulting from the lyophobic and lyophilic regions, induced capillary effects that guided the nucleation and growth of perovskite crystals. As the solvent evaporated, the precursor concentration increased, leading to supersaturation and subsequent crystal nucleation within the micropillar structures.
4. **Formation of 1D $CsPbBr_3$ Arrays:** The controlled environment provided by the micropillar template, and the confined precursor solution ensured the formation of highly ordered 1D $CsPbBr_3$ arrays on the substrate. These arrays were

characterized by uniform size and alignment, which are crucial for their application in optoelectronic devices.

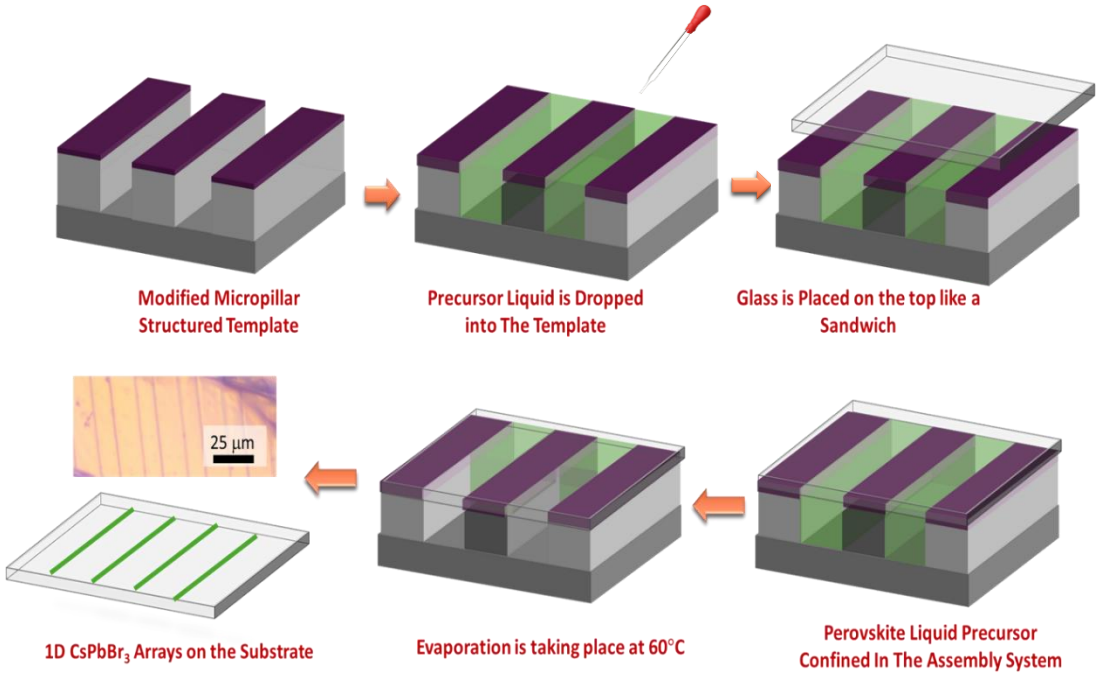

Figure 4.2: Schematic representation of the patterning synthesis process for lead halide perovskites using a modified micropillar structured template. The process involves dropping a 0.3M precursor solution onto the template, covering it with a glass or silicon substrate, and allowing evaporation to occur at 60°C for 24 hours. The asymmetric wettability of the template guides the nucleation and growth of highly ordered 1D $CsPbBr_3$ and $CsPb_2Br_5$arrays, resulting in precise and uniform perovskite structures.

Results and Discussion

In this section, we present a detailed analysis of the patterned synthesis of cesium lead bromide perovskites, specifically $CsPbBr_3$ and $CsPb_2Br_5$, using trench and nanohole templates. The successful formation of these highly ordered perovskite structures was confirmed through photoluminescence (PL) for $CsPbBr_3$ and Raman spectroscopy for CsPbBr5. The analysis highlights the effectiveness of our synthesis approach and provides insights into the structural and optical properties of the resulting crystals.

Synthesis and Characterization of $CsPbBr_3$

The synthesis of $CsPbBr_3$ was extensively analyzed using photoluminescence (PL) spectroscopy. The microscopic images of $CsPbBr_3$ reveal well-defined and continuous lines of crystals within the trench templates. These images, captured at various magnifications, show that the crystal growth was effectively guided by the template, resulting in uniform distribution and alignment along the trenches. The first set of

microscopic images shows the trench pattern, where the perovskite crystals are precisely confined within the trench structures. The crystals exhibit a high degree of uniformity and alignment, indicating successful patterning and growth.

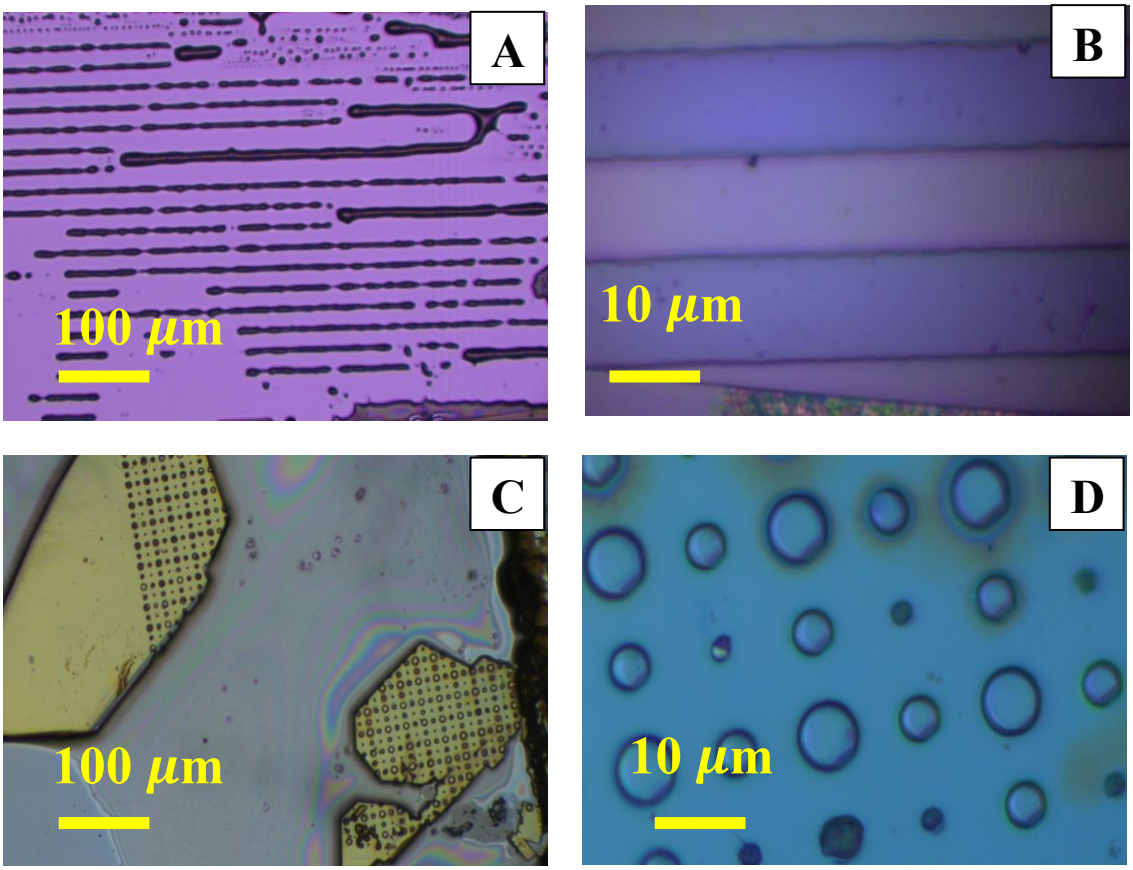

Figure 4.3: Microscopic images of the patterned synthesis of cesium lead bromide perovskites ($CsPbBr_3$). (A) Trench pattern at 10X magnification, showing continuous and well-aligned lines of $CsPbBr_3$ crystals. (B) Trench pattern at 100X magnification, providing a detailed view of the uniformity and alignment within the trenches. (C) Nanohole pattern at 10X magnification, displaying a regular array of uniformly sized and distributed $CsPbBr_3$ crystals confined within the nanohole structures. (D) Nanohole pattern at 100X magnification, highlighting the high precision and regularity of crystal growth.

The photoluminescence (PL) spectra of $CsPbBr_3$ exhibited strong and consistent emission peaks, indicative of the high quality of the perovskite crystals synthesized. The intensity and sharpness of the PL signals suggest a minimal presence of defects within the crystal structure, highlighting the high crystallinity of the synthesized $CsPbBr_3$. These emission peaks were observed at a wavelength of approximately 525 nm, which is characteristic of $CsPbBr_3$, confirming the successful formation of the desired perovskite phase.

Such optical properties are paramount for applications in optoelectronic devices, where the performance is heavily dependent on the quality and defect-free nature of the perovskite materials. The excitation laser used for the analysis was at a wavelength of 405 nm, ensuring efficient excitation of the perovskite material to reveal its photoluminescent properties.

Notably, this analysis was conducted on bulk crystals of $CsPbBr_3$, further demonstrating the material's robustness and high quality in its macroscopic form.

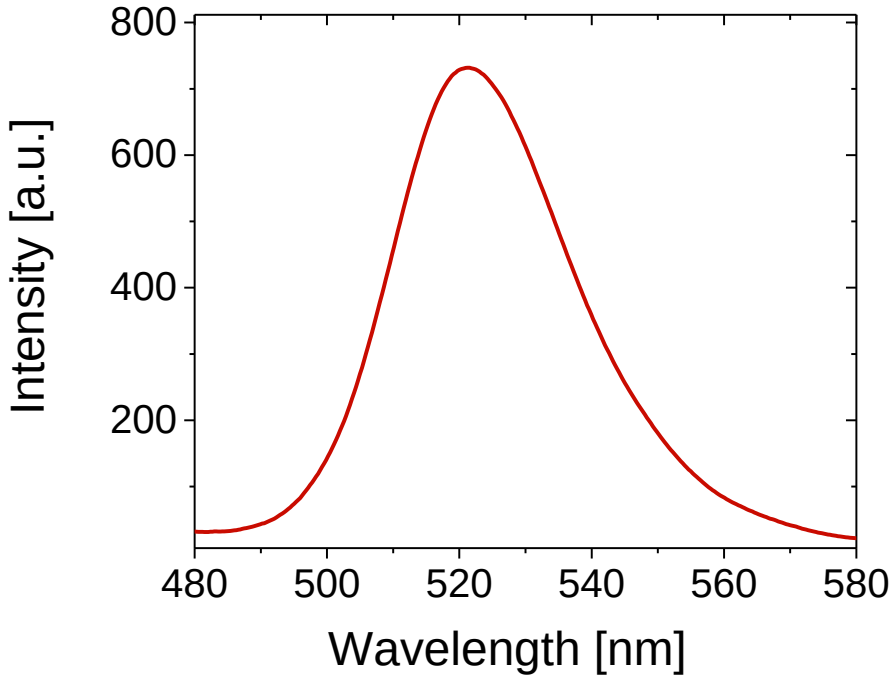

Figure 4.4: Photoluminescence (PL) spectrum of $CsPbBr_3$ perovskite crystals, showing a strong emission peak at approximately 525 nm.

Synthesis and Characterization of $CsPb_2Br_5$

The synthesis of $CsPb_2Br_5$ was validated using Raman spectroscopy. The microscopic images show uniformly distributed $CsPb_2Br_5$ crystals within the nanohole templates. The images highlight the regularity and precision of the crystal growth within the nanoholes, demonstrating the effective control over nucleation and growth processes provided by the template. The nanohole pattern images display a regular array of $CsPb_2Br_5$ crystals, with each crystal precisely confined within the nanohole structures.

Raman spectroscopy provided detailed insights into the structural properties of $CsPb_2Br_5$. The Raman spectra exhibited characteristic peaks corresponding to the vibrational modes of $CsPb_2Br_5$, specifically at B_1g, B_2g, A_1g, and Eg modes.[13]

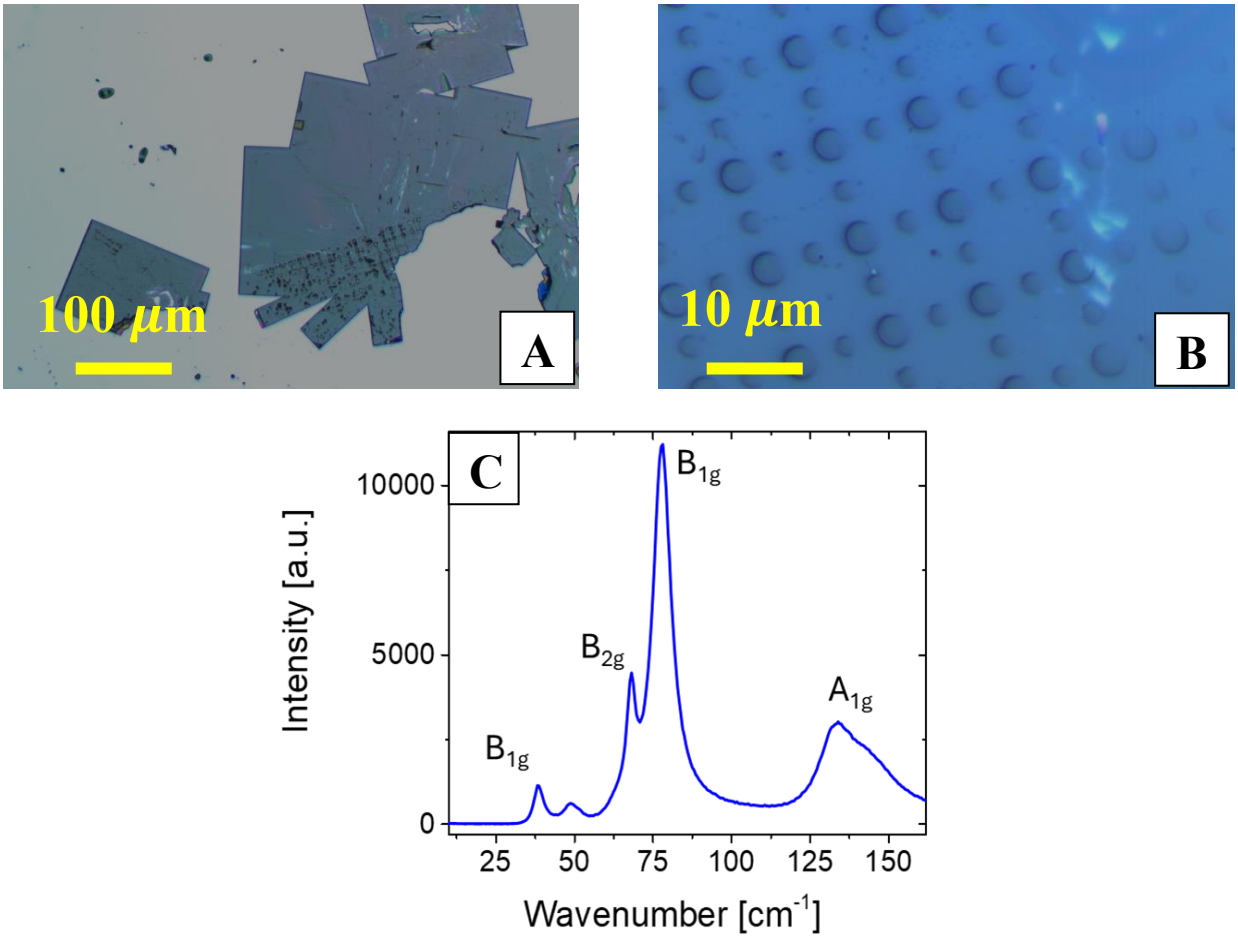

Figure 4.5: Characterization of $CsPb_2Br_5$ perovskite crystals synthesized using nanohole templates. (A) Microscopic image with 10X magnification highlighting the uniform distribution and size of CsPbBr5 crystals within the nanohole templates. (B) Microscopic image with 100X magnification showing a regular array of CsPbBr5 crystals precisely confined within the nanohole structures, demonstrating successful patterning and controlled crystal growth. (C) Raman spectrum of CsPbBr5, displaying characteristic peaks at vibrational modes B_1g, B_2g, A_1g, and Eg, confirming the formation of high-crystallinity CsPbBr5 perovskite with minimal impurities.

The presence of these modes confirms the formation of the desired perovskite phase. The sharp and well-defined peaks indicate high crystallinity and minimal impurities within the crystals. The successful identification of $CsPb_2Br_5$ through its Raman spectral features demonstrates the structural integrity and quality of the synthesized crystals. These structural properties are vital for applications that require stable and well-ordered perovskite materials.

Analysis of Photoluminescence Spectra in Relation to Precursor Concentrations

We investigated the effects of varying the molar ratios of CsBr to $PbBr_2$ on the formation of We investigated the effects of varying the molar ratios of CsBr to $PbBr_2$ on the formation of $CsPbBr_3$ and $CsPb_2Br_5$. Figure 4.6 shows the normalized PL spectra of $CsPbBr_3$ synthesized using different precursor ratios (1:1, 1:2,1:2.5, 1:3, 1:4 and 1:5). The photoluminescence (PL) spectra of $CsPbBr_3$ crystals synthesized with varying molar ratios of CsBr to $PbBr_2$ provide insights into their structural and optical properties. The table outlines the specific molar ratios and precursor concentrations used in the synthesis, while the PL spectra illustrate the impact of these ratios on the resulting crystals.

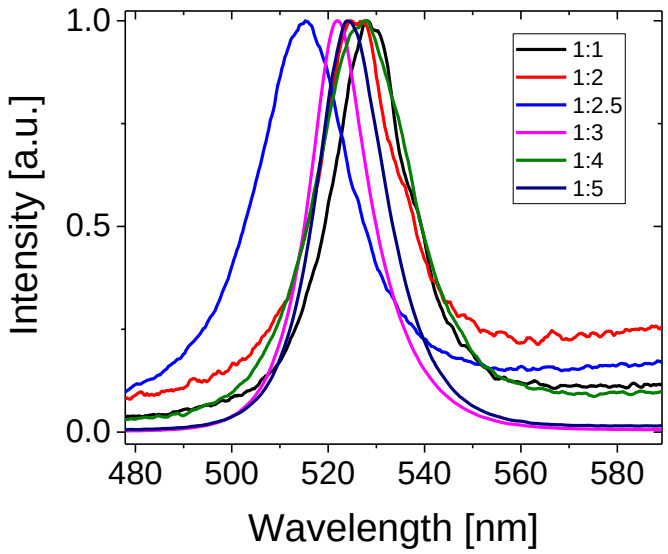

Figure 4.6: Photoluminescence Spectra of $CsPbBr_3$ Crystals Synthesized with Different Molar Ratios of CsBr to $PbBr_2$.The figure shows the normalized photoluminescence (PL) spectra of $CsPbBr_3$ crystals synthesized with varying molar ratios of CsBr to $PbBr_2$. The molar ratios tested include 1:1, 1:2, 1:2.5, 1:3, 1:4, and 1:5. The PL peaks are centered around 515-529 nm, indicating the formation of the $CsPbBr_3$ phase. The intensity and slight shifts in the peak positions reflect changes in crystal quality and composition.

For the 1:1 molar ratio of CsBr to $PbBr_2$, the PL spectrum shows a peak centered around 528 nm, indicating the formation of $CsPbBr_3$. The relatively broad emission peak suggests the presence of some defects. Increasing the ratio to 1:2 maintains the peak at 526 nm, indicating that $CsPbBr_3$ remains the primary phase.

At a 1:2.5 ratio, the PL spectrum shows a peak around 515 nm, suggesting improved crystal quality and fewer defects compared to the lower ratios. The 1:3 ratio results in a slight shift of the PL peak to 521.8 nm, indicating subtle changes in the crystal structure or composition.

The 1:4 molar ratio exhibits a PL peak at 526.8 nm observed, suggesting optimal conditions for high-quality $CsPbBr_3$ crystal growth. This high intensity reflects enhanced optical properties and better crystallinity. At the 1:5 ratio, the PL spectrum still shows a peak around 525 nm. However, this observation may indicate a potential increase in defect states or slight deterioration in crystal quality at this higher precursor concentration.

CsBr (g)	**$PbBr_2$(g)**	**Ratio**	**Total Molarity**	**Dominant Phase**	**PL Peak Center**
0.02128	0.036701	1:1	0.1M	$CsPbBr_3$	528.7 nm
0.02128	0.073402	1:2	0.14M	$CsPbBr_3$	526.0 nm
0.02128	0.091753	1:2.5	0.17M	$CsPbBr_3$	514.9 nm
0.02128	0.110103	1:3	0.21M	$CsPbBr_3$	521.8 nm
0.02128	0.146804	1:4	0.24M	$CsPbBr_3$	526.8 nm
0.02128	0.183505	1:5	0.3M	$CsPbBr_3$	524.3 nm
0.02128	0.220206	1:6	0.35M	$CsPb_2Br_5$	No PL

Table 4.1: Precursor Concentrations and Varying Molar Ratios for the Synthesis of $CsPbBr_3$ and $CsPb_2Br_5$ Crystals

As the ratio of $PbBr_2$ increases beyond 1:5, the formation of $CsPbBr_3$ starts to decline, and another phase, $CsPb_2Br_5$, begins to form (Table 4.1). At a 1:6 molar ratio of CsBr to $PbBr_2$, Raman spectroscopy confirmed the successful synthesis of $CsPb_2Br_5$. The characteristic Raman peaks corresponding to $CsPb_2Br_5$ validate the presence of this perovskite phase, indicating a structural shift due to the higher concentration of $PbBr_2$.

Notably, while previous studies such as those by Feng et al. have reported the successful patterning and synthesis of $CsPbBr_3$, no other groups have reported achieving a patterned synthesis of $CsPb_2Br_5$. Our study is the first to demonstrate the patterned synthesis of $CsPb_2Br_5$, marking a significant advancement in the field of perovskite research. The high crystallinity and precise control over crystal growth achieved in our study pave the way for further exploration and optimization of patterned $CsPb_2Br_5$ for various advanced applications.

Chapter 5: Conclusion and Future Directions

This thesis has made significant strides in addressing the key challenges associated with the synthesis, characterization, and patterning of lead halide perovskites (LHPs) for advanced photonic applications. Through the development of an innovative synthesis method that integrates soft lithography with self-assembly, this work has demonstrated the feasibility of creating highly ordered and stable LHP structures.

Key Contributions

1. **Advancements in LHP Synthesis:** The novel synthesis approach combining soft lithography and self-assembly successfully addressed the limitations of traditional methods. This technique enabled precise control over the nucleation and growth of LHP crystals by using a patterned template with asymmetric wettability. The resulting LHP structures exhibited high crystallographic order, essential for optimal performance in optoelectronic devices.
2. **Successful Patterning of $CsPbBr_3$ and $CsPb_2Br_5$:** The study validated the patterned synthesis of $CsPbBr_3$ and $CsPb_2Br_5$. Photoluminescence (PL) spectroscopy confirmed the high optical quality of $CsPbBr_3$, with strong emission peaks around 525 nm indicating minimal defects. Raman spectroscopy of $CsPb_2Br_5$ revealed characteristic peaks corresponding to the B_1g, B_2g, and A_1g, vibrational modes, confirming the formation of the desired perovskite phase with high crystallinity. Notably, this work is the first to achieve the patterned synthesis of CsPbBr5, representing a significant breakthrough.
3. **Microscopic Characterization:** Microscopic images demonstrated the successful patterning of $CsPbBr_3$ and $CsPb_2Br_5$ within trench and nanohole templates. The regular and uniform distribution of crystals within these patterns highlighted the effectiveness of the proposed synthesis method in controlling crystal growth.

Implications and Future Directions

The findings of this thesis have profound implications for the future development of LHP-based photonic devices. The ability to pattern LHPs with high precision and control opens new possibilities for their integration into sophisticated optoelectronic applications. This method provides a scalable and practical solution to the challenges of stability and patterning, potentially accelerating the commercialization of LHPs in various technologies.

Future research could build on these results by exploring the integration of patterned LHP structures into functional devices, such as light-emitting diodes, lasers, and photodetectors. Additionally, further optimization of the synthesis process and exploration of other LHP compositions could expand the applicability and enhance the performance of these materials.

This thesis has advanced the field of lead halide perovskites by developing a novel and effective synthesis method that overcomes significant challenges related to stability and patterning. The successful patterned synthesis of $CsPbBr_3$ and $CsPb_2Br_5$, particularly the unprecedented achievement with $CsPb_2Br_5$, underscores the potential of LHPs for next-generation photonic devices. This work lays a solid foundation for future research and development, contributing to the broader goal of harnessing the exceptional properties of LHPs for innovative optoelectronic applications.

References

[1] Liu, J. (2020). Synthesis, Self-assembly, and Regrowth of Lead Halide Perovskite Nanocrystals. KAUST Research Repository.DOI: [10.25781/KAUST-8RHU8] (https://doi.org/10.25781/KAUST-8RHU8)

[2] Deng, Y. H., Xiao, Z. G., & Huang, J. S. (2023). Metal Halide Perovskite for Next-Generation Optoelectronics: Progresses and Prospects. eLight.DOI: [10.1002/adma.202000597] (https://doi.org/10.1002/adma.202000597)

[3] Zhang, Y., Deng, Y. H., Xiao, Z. G., & Huang, J. S. (2023). Direct Laser Writing on Halide Perovskites: From Mechanisms to Applications. Light: Advanced Manufacturing. DOI: [10.1002/admt.202200275] (https://doi.org/10.1002/admt.202200275)

[4] Snaith, H. J. (2013). Perovskites: The Emergence of a New Era for Low-Cost, High-Efficiency Solar Cells. The Journal of Physical Chemistry Letters, 4(21), 3623–3630. DOI: [10.1021/jz4020162] (https://doi.org/10.1021/jz4020162)

[5] Qu, J., Xu, S., Shao, H., Xia, P., Lu, C., Wang, C., & Ban, D. (2023). Recent Progress of Copper Halide Perovskites: Properties, Synthesis, and Applications. Journal of Materials Chemistry C.DOI: [10.1039/D3TC00503H] (https://doi.org/10.1039/D3TC00503H)

[6] Harwell, J., et al. (2019). Patterning Multicolor Hybrid Perovskite Films via Top-Down Lithography. ACS Nano.DOI: [10.1021/acsnano.8b09592] (https://doi.org/10.1021/acsnano.8b09592)

[7] Nayak, P. K., et al. (2019). Perovskite Light-Emitting Diodes Toward Commercial Full-Colour Displays. Advanced Materials. DOI: [10.1002/adma.201900279](https://doi.org/10.1002/adma.201900279)

[8] Dou, L. T., et al. (2017). Spatially Resolved Multicolor CsPbX3 Nanowire Heterojunctions via Anion Exchange. Proceedings of the National Academy of Sciences. DOI: [10.1073/pnas.1617810114](https://doi.org/10.1073/pnas.1617810114)

[9] Wang, Y., et al. (2019). Perovskite-Ion Beam Interactions: Toward Controllable Light Emission and Lasing. ACS Applied Materials & Interfaces. DOI: [10.1021/acsami.9b03298] (https://doi.org/10.1021/acsami.9b03298)

[10] Gu, Z. K., et al. (2020). Controllable Growth of High-Quality Inorganic Perovskite Microplate Arrays for Functional Optoelectronics. Advanced Materials.DOI: [10.1002/adma.201908006](https://doi.org/10.1002/adma.201908006)

[11] Zhang, Zhaojun, et al. (2018). Growth, Characterization, and Optoelectronic Applications of Pure-Phase Large-Area CsPb2Br5 Flake Single Crystals. Journal of Materials Chemistry C, 6(3), 446-451. DOI: [10.1039/C7TC05276A](https://doi.org/10.1039/C7TC05276A)

[12] Feng, Jiangang, et al. (2017). Crystallographically Aligned Perovskite Structures for High-Performance Polarization-Sensitive Photodetectors. Advanced Materials, 29(16), 1605993. DOI: [10.1002/adma.201605993] (https://doi.org/10.1002/adma.201605993)

[13] Hadjiev, V. G., Wang, C., Wang, Y., Su, X., Calderon, H. A., Hernandez, F. R., Wang, Z. M., Bao, J. M. (2018). Phonon Fingerprints of CsPb2Br5. Journal of Physics: Condensed Matter, 30(40), 405703.DOI: [10.1088/1361-648X/aadb96](https://doi.org/10.1088/1361-648X/aadb96)

[14] Yin, Jun, Haoze Yang, Kepeng Song, Ahmed M. El-Zohry, Yu Han, Osman M. Bakr, Jean-Luc Brédas, and Omar F. Mohammed. "Point defects and green emission in zero-dimensional perovskites." *The Journal of Physical Chemistry Letters*, 9(18), 5490-5495. (2018).

[15] Zhou, Bo, et al. "A scalable H2O–DMF–DMSO solvent synthesis of highly luminescent inorganic perovskite-related cesium lead bromides." *Advanced Optical Materials* 9.3 (2021): 2001435.

[16] Zhang, Zhaojun, et al. "Thermal decomposition mechanism of $CsPb_2Br_5$ single crystals." Journal of Materials Chemistry C 6.3 (2018): 446-451

[17] Liu, Yuling, et al. "Chemical transformation mechanism for blue-to-green emitting $CsPbBr_3$ nanocrystals." Nanoscale 16 (2024): 6507-6515. DOI: 10.1039/D3NR05215J.

[18] Yun, Rui, et al. "Mixed-Solvent Polarity-Assisted Phase Transition of Cesium Lead Halide Perovskite Nanocrystals with Improved Stability at Room Temperature." Nanomaterials 9.11 (2019): 1537. DOI: 10.3390/nano9111537

[19] Jiang, S. et al. "Photo-induced structural and optical changes of $CsPbBr_3$ perovskite nanocrystals." Journal of Materials Chemistry A, 2020, 8, 14015-14022. DOI: 10.1039/D0TA04155F

[20] Abu Bakar, M. R., Nagy, Z. K., Saleemi, A. N., & Rielly, C. D. "The Impact of Direct Nucleation Control on Crystal Size Distribution in Pharmaceutical Crystallization Processes." Crystal Growth & Design, 2009, 9(3), 1378-1384